

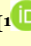




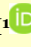
Rockfall localization from seismic polarization considering multiple triaxial geophones and frequency bands


Liang FENG^{1,2*}  <https://orcid.org/0000-0002-6975-2759>;  e-mail: liang.feng@unifi.it

Veronica PAZZI¹  <https://orcid.org/0000-0002-9191-0346>; e-mail: veronica.pazzi@unifi.it

Emanuele INTRIERI¹  <https://orcid.org/0000-0002-9227-4409>; e-mail: emanuele.intrieri@unifi.it

Teresa GRACCHI¹  <https://orcid.org/0000-0002-8838-2693>; e-mail: teresa.gracchi@unifi.it

Giovanni GIGLI¹  <https://orcid.org/0000-0003-4317-5882>; e-mail: giovanni.gigli@unifi.it

Grazia TUCCI¹  <https://orcid.org/0000-0001-7657-9723>; e-mail: grazia.tucci@unifi.it

**Corresponding author*

1 Department of Earth Sciences, University of Florence, Via G. La Pira 4, 50121 Florence, Italy

2 Department of Civil and Environment Engineering, University of Florence, Via Santa Marta 3, 50139 Florence, Italy

Citation: Feng L, Pazzi V, Intrieri E, et al. (2020) Rockfall localization from seismic polarization considering multiple triaxial geophones and frequency bands. *Journal of Mountain Science* 17(7). <https://doi.org/10.1007/s11629-020-6132-1>

Abstract: Boulder/rock mass movements generate ground vibrations that can be recorded by geophone networks. Generally, there are two methods applied to rockfall trajectory reconstruction or rockfall seismic localization. One method uses seismic wave arrival times and is achieved by minimizing the differences in signal arrival times between multiple stations by grid map searching. The other method uses seismic polarization and is achieved by calculating event-source back azimuths from the seismic polarizations of rockfall signals. In this study, we proposed the use of an overdetermined matrix for joint localization based on the polarization method. The overdetermined matrix considers the contributions of all geophones in the network, and at each geophone is assigned a different weight according to the recorded signal qualities and the reliability of the calibrated back azimuths. This method shows a great advantage relative to the case in which only two sensors are employed. Besides, we suggested three marker parameters for proper frequency band selection in

back azimuth calculations: energy, rectilinearity, and a special permanent frequency band (SPF). We found that the back azimuths calculated with energy and an SPF are generally close to the real back azimuths measured in the field, while the SPF is limited by seismic attenuation due to a long-distance propagation. The localization results of rockfalls were validated by using field camera videos and in situ calibrations. Three typical cases and 43 artificially released rockfalls are presented in this paper. The proposed method provides an interesting way to locate rockfall events and track rockfall trajectories and avoids the difficulties of obtaining accurate arrival times, as required by the arrival times method.

Keywords: Rockfall; Localization; Seismic polarization; Seismic monitoring; Early warning

Introduction

Landslides are ubiquitous in terrestrial environments with slopes and are driven by

tectonics, climate and/or human activities. Rockfalls, one of the major landslide hazards, are characterized by intermittent and rapid mobilization, various types of sliding, and volumes (Hung et al. 2014). They are difficult to forecast and/or predict. Unobserved rockfall pose a significant risk to people and transportation, such as the T179 train derailment accident occurred on March 2020, in the city Chenzhou, China, that was induced by an unobserved small landslide deposited on the railway. Seismic monitoring of landslides allows to collect vast amounts of important information able to characterize the events (e.g., event-types, energies, durations, localizations, and the processes of event development) (Deparis et al. 2008; Vilajosana et al. 2008; Helmstetter and Garambois 2010; Hibert et al. 2011; Coviello et al. 2019; Pazzi et al. 2019; Zhang et al. 2019; Zhang et al. 2020). This method could be popularly employed thanks to the cheap price of instruments. For slope stability evaluation, it is useful and practical to determine susceptible slope areas as soon as the localizations of the seismic events (e.g., crack breaking and rockfall) are found. This information could be also employed in transportation early warning systems, where the dangerous could be fast alarmed as soon as rockfalls and/or landslides occurred. Early warning systems (EWS), in fact, have been addressed by United Nations International Strategy for Disaster Reduction as powerful tool to reduce risks for a vast range of threats, including landslides, and the localization of seismic event is a dispensable part of an EWS. Seismic localization is commonly used in earthquake and has also been developed for volcanic, bombing, and geohazard non-tectonic events (Kao et al. 2004; Vilajosana et al. 2008; Guinau et al. 2019).

Seismic polarization (polarization-bearing, P-B in the following), is a method of localization, commonly used in earthquake, that deals with seismic source back azimuth calculations by means of the analysis of the seismic polarization of the signals recorded by three-component geophones (Flinn 1965; Samson and Olson 1980; Vidale 1986; Magotra et al. 1987; Jurkevics 1988). This method requires that the seismic signal is only composed of *P*-wave, so that the direction of polarization is the direction of the source. At present, Vilajosana et al. (2008) extended the P-B technique to an artificially

triggered rockfall by using two three-component seismic stations located at the foot of the Montserrat massif approximately 200 m from the rockfall explosion point. They calculated the seismic polarization of the trace of the first block that fell onto the terrace, and the estimated propagation velocity was in a good agreement with the measured *P*-wave velocity. There are also many other methods applied in seismic localization, such as the method of arrival times based on the shortest-path method that minimizes the differences among seismic signal first-arrival times recorded by multiple stations and gridded topographic map searching (Moser et al. 1992; Rodi et al. 2000; Jolly et al. 2002; Kao et al. 2004; Dammeier et al. 2011; Lacroix and Helmstetter 2011; Xu et al. 2011; Lacroix et al. 2012; Gracchi et al. 2017) and the method of beam-forming by combining the time-shift resulting in the maximum stacked amplitude of the signals and the positions of the sensors through map grid-searching (Rost and Thomas 2002; Heck et al. 2019). The method of arrival times is easily understood and widely applied, but the localization precision is heavily dependent on the accuracy of picking the first-arrival times, especially for near-field microseismic monitoring, such as rockfall and/or landslide monitoring. Moreover, the seismic wave attenuation and propagation velocities are influenced by topography, lithology, and geological formations that strongly influence high-accuracy picking of the first-arrival times (Kao et al. 2004). In P-B, the localization is carried out by using the seismic signal polarization, so the accuracy requirement for picking arrival times is not as strict as the method of arrival times. The main problem of the P-B method is the determination of the *P*-phase and the correct frequency bands for polarization and back-azimuth calculations from the recorded time series.

Both the traces from an artificially released rockfall test performed in a limestone quarry and recorded by four geophones as well as the videos from four monitoring cameras were available. Starting with the P-B method drawbacks mentioned above (e.g., frequency band selection and multi-station joint localization), we decided to use these data to attempt to define marker parameters that would indicate the most appropriate frequency bands for calculations of

seismic polarization and back azimuths. Moreover, to use the signals recorded by all geophones deployed in the network, an overdetermined matrix was proposed for joint localization based on signal record quality and energy.

1 Material and Methods

1.1 Study area and data acquisition

The seismic instruments employed in this study are four three-component geophones (S45 triaxial velocimeter) produced by the SARA Electronic Instrument company. The natural frequency of these instruments is 4.5 Hz, and they were connected by means of cable to a 24-bit digitizer, that continuously recorded seismic waves in three directions (e.g., east-west direction – E, north-south direction – N, and vertical direction – Z). They acquired data at a sampling rate of 200 Hz. The localizations of the four geophones (TOR 1, TOR 2, TOR 3, and TOR 4) installed as a seismic monitoring network are shown in Figure 1. This monitoring network, placed in the upper part of a former quarry, Torgiovanetto, is located 2 km northeast of the city of Assisi (Central Italy), and the former quarry contains 182,000 m³ of unstable rock mass. More information about this test site, the seismic network, and the seismic signal characteristics can be found in previous studies by Lotti et al. (2014), Lotti et al. (2018), Feng et al. (2019, 2020). Moreover, in Gracchi et al. (2017), the methodology of arrival times for a fast and practical localization was utilized to locate rockfall events on the basis of 90 controlled-release limestone blocks, and its performance in locating the events was presented.

To better evaluate the performance of the P-B method, one of the rockfalls released during the tests, N.39 (its localization is shown in Figure 1 as a white star), was chosen thanks to its clear signals and video recordings. The rockfall N.39 seismic signals and spectrograms, recorded by the four geophones, are shown in Figure 2. The localization estimation was performed only for the first impact onto the slope surface. The signal of the first impact is shown between the two vertical red dashed lines (in the following marked as rockfall N.39-impact #1).

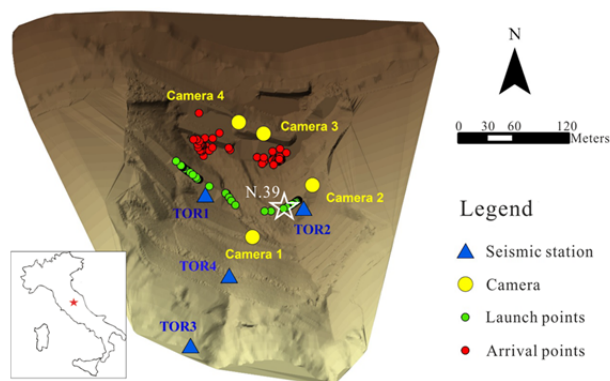


Figure 1 The Digital Elevation Model (DEM) of the seismic monitored site, the site location was shown in the map of Italy as a red star. The white starred point is the starting position of rockfall N.39.

For back azimuth calculations and polarization processing, bandpass filters are employed to analyse the three-component seismograms. The choice of bandwidth of frequency band is subject to the usual trade-offs between resolution and estimation variance. Narrow bands are required to avoid smearing information to capture the frequency-varying properties of polarization, while wider frequency bands yield more stable and reliable estimates (Jurkevics 1988). For this reason, some kind of spectral balancing is needed by computing separate covariance matrices in a series of narrow frequency bands, and then normalizing and averaging. In this study, the fixed narrow bandwidth was set to 1 Hz, that's enough to smooth particle movement, and more widely frequency bands can be obtained by normalizing and averaging them. Moreover, short time windows are selected to analyse signals corresponding to single seismic events. However, the length of the time window and the frequency bands of the *P*-wave are controlled by the event duration and the event type, respectively.

1.2 Overdetermined matrix and weight assignments for joint localization

The seismic polarization methodology refers to the studies by Jurkevics (1988) and Vilajosana (2008), based on bandpass filtering. In this section, we will focus on the seismic station differential judgement by using an overdetermined matrix and weight to more than two stations for joint localization. For the case of two geophones, an event localization can easily be obtained by

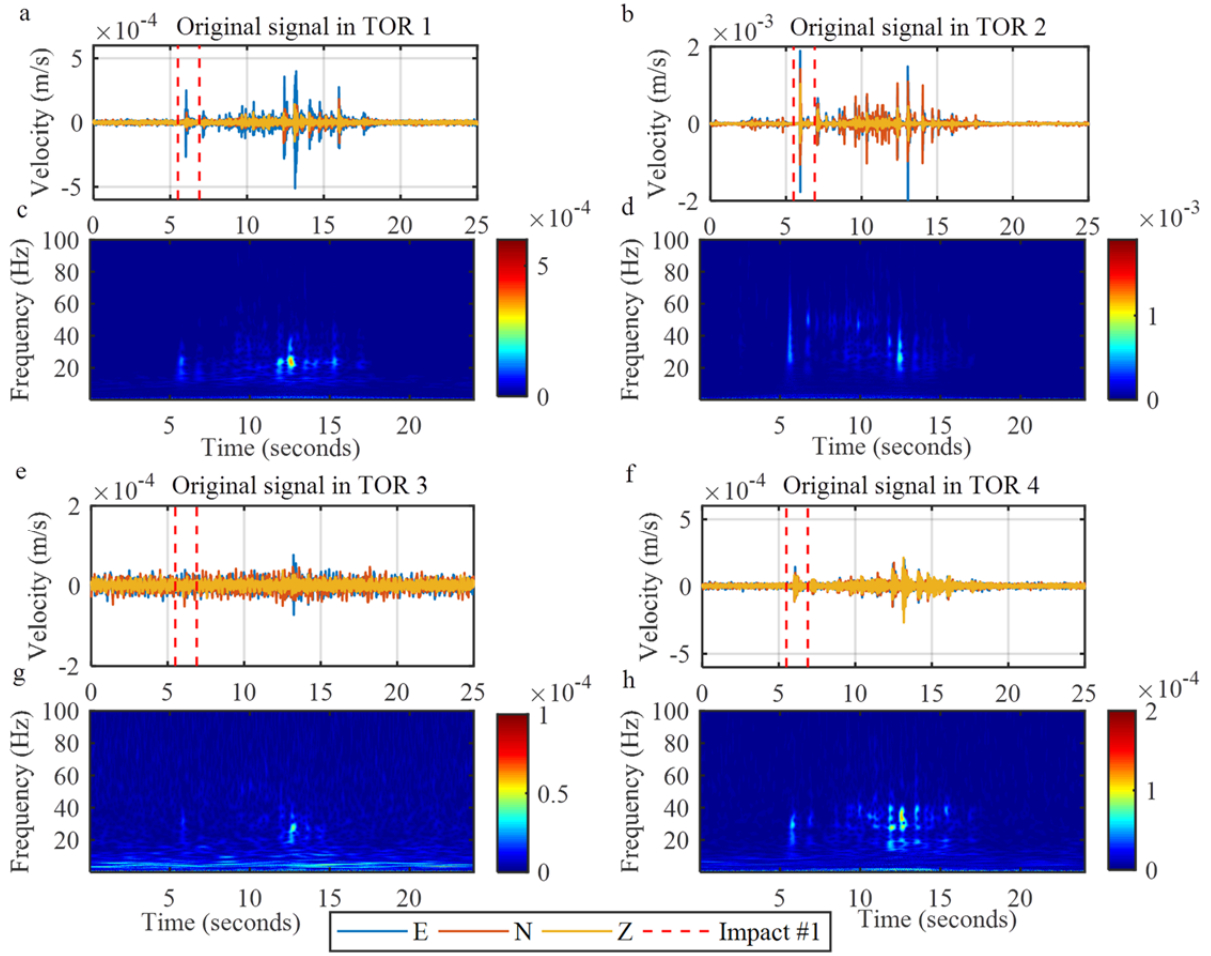


Figure 2 Original signals recorded at four seismic stations (a, b, e, f) and their spectrograms of signals recorded by East-component (c, d, g, h); in figures, the short portion of the signal between the two red dashed lines is rockfall N.39-impact #1, and the color bar is intensity with unit of velocity (m/s).

calculating two-point positions and their unparallel back azimuths. In practice, the errors in back azimuth calculations and incorrect frequency band choices limit precise localization when utilizing only two geophones. To obtain a more accurate result, more than two stations are required in a seismic monitoring network. Moreover, in multi-station monitoring practice, the signal quality and the reliability of the back azimuths used are different from one station to the next, given wave propagation attenuation, geomorphology, and the recorded signal intensity. For example, as shown in Figure 2, the signal intensity at TOR 3 is significantly weaker than for the other stations. Therefore, in P-B localization with multiple joint stations, mutual calibration is necessary.

Assuming that the back azimuths estimated in a horizontal plane are θ_s , the event location is (\bar{x}_s, \bar{y}_s) , and the position of seismic station (s) is

(x_s, y_s) . Therefore, at seismic station s , the analytical localization equation will be:

$$\tan(\theta_s) = \frac{\bar{y}_s - y_s}{\bar{x}_s - x_s} \quad (1)$$

and its matrix expression will be:

$$[-\tan(\theta_s), 1] \begin{bmatrix} \bar{x}_s \\ \bar{y}_s \end{bmatrix} = y_s - x_s \tan(\theta_s) \quad (2)$$

When more than two stations (S_1, S_2, S_3, S_4) are employed in a monitoring network, as shown in Figure 3, the analytical localization equation can be presented as the overdetermined matrix shown in Eq. 3:

$$Mx = N \quad (3)$$

$$\text{where } M = \begin{bmatrix} -\tan(\theta_1) & 1 \\ -\tan(\theta_2) & 1 \\ -\tan(\theta_3) & 1 \\ -\tan(\theta_4) & 1 \end{bmatrix}, N = \begin{bmatrix} y_1 - x_1 \tan(\theta_1) \\ y_2 - x_2 \tan(\theta_2) \\ y_3 - x_3 \tan(\theta_3) \\ y_4 - x_4 \tan(\theta_4) \end{bmatrix}$$

$$x = \begin{bmatrix} \bar{x}_1 & \bar{x}_2 & \bar{x}_3 & \bar{x}_4 \\ \bar{y}_1 & \bar{y}_2 & \bar{y}_3 & \bar{y}_4 \end{bmatrix}.$$

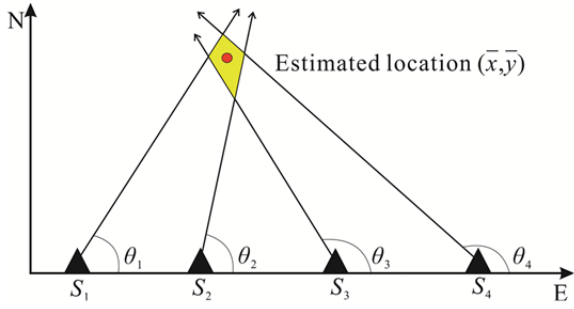


Figure 3 General sketch for the localization by means of multiple seismic stations. In picture, the yellow area is crossed by back azimuths that event probably located, and the red point is the optimal event location.

Therefore, the optimal result for the event localization (\bar{x}, \bar{y}) will be the solution of the overdetermined matrix shown in Eq. 3, calculated as follows:

$$\begin{bmatrix} \bar{x} \\ \bar{y} \end{bmatrix} = \operatorname{argmin}((Mx - N)^T(Mx - N)) \quad (4)$$

where, argmin is the function's minimum value of x .

Furthermore, considering that signal intensity and quality are different among stations, a weight is assigned to each station in the overdetermined matrix calculation. The weight is calibrated based on the seismic energy of the analysed signal recorded at each station, i.e., higher signal energy indicates higher reliability for the calculated back azimuth and a higher weight assigned. Moreover, when the signal energy is below the noise level, the weight is set to 0, and the station is not considered in the calibration of back azimuths. It is important to note that, the employed energy is a relative quantity and not an absolute quantity because it is calculated as the sum of squared amplitude at each station, as same as the energy (E) defined in section 1.3.1. Thus, factors such as attenuation effects and geometrical spreading are not included, and the chance of introducing processing errors is reduced (Dammeier et al. 2011).

The weights, defined as (w_1, w_2, w_3, w_4) , for four seismic stations, form a matrix:

$$\mathbf{W} = \begin{bmatrix} w_1 & 0 & 0 & 0 \\ 0 & w_2 & 0 & 0 \\ 0 & 0 & w_3 & 0 \\ 0 & 0 & 0 & w_4 \end{bmatrix} \quad (5)$$

Finally, combining the overdetermined and weight matrices, the improved event source localization (\hat{x}, \hat{y}) is:

$$\begin{bmatrix} \hat{x} \\ \hat{y} \end{bmatrix} = \operatorname{argmin}((Mx - N)^T W(Mx - N)) \quad (6)$$

In addition, we usually obtain event localizations on a horizontal plane, but when the altitude of a rockfall induced seismic event is required, it can be determined by projecting the horizontal coordinates onto a 3D topographic map to find the correct altitude value. However, this approach is not working when the slope is steep.

1.3 Marker parameters for frequency band selections

To locate rockfalls by means of the P-B method, the detailed seismic wave mode of the rockfall signal has to be known and the appropriate frequency bands, for which the particle movement is in the direction of propagation (e.g., the P -wave), has to be determined. From the studies of Kao et al. (2012), the seismic characteristics of the landslide and mud/debris flow (LMDF) waveforms are significantly different from those of earthquakes. In fact, for rockfall detected in the near-field, LMDF signals are sharp and are characterized by irregular P/S bursts related to the landslide history. After a careful examination of all LMDF waveforms that were recorded in Taiwan by a broadband array in a seismograph network, the authors suggested the P and S -phases intermix as a robust feature to distinguish LMDF events and some particularly stronger bursts (mostly corresponding to P -waves) have slightly richer spectral contents (Kao et al. 2012). Therefore, three marker parameters, energy (E), rectilinearity (I), and a special permanent frequency (SPF), were analysed in this study to determine the appropriate frequency bands for P -wave for seismic polarization and back azimuth calibration.

1.3.1 Energy (E)

To evaluate the usefulness of energy as marker parameter, the energy and back azimuth of each bandpass filtered signal from rockfall N.39-impact #1 were calculated, and the back azimuths were then compared with the in-situ measurements to determine the correct frequency bands and their relationships with energy.

The signal from rockfall N. 39-impact #1 was bandpass filtered into 96 frequency bands, each with a width of 1 Hz and ranging from 3 Hz to 99

Hz. The frequencies (0 Hz–3 Hz) and the frequency band (99 Hz – 100 Hz) were discarded since noise dominated and there were filter and recording errors (Feng et al. 2019). For each of the 96 frequency bands evaluated, the back azimuths and the FFTA (fast Fourier transform coefficient) were calculated. The FFTA values represent the energy of a signal in a given frequency band as defined by Feng et al. (2019). Figure 4 is a plot of the results. Moreover, the back azimuths measured in situ as illustrated in Gracchi et al. (2017) and referred to here as “real back azimuth” are also shown (dashed blue line) in Figure 4.

The results show that the back azimuths calculated from the frequency bands from 15 Hz – 45 Hz are mainly close to the real back azimuth, and in parallel, the energies in the frequency bands from 20 Hz – 40 Hz have the most energy in the full-frequency bands. This rule is valid for all rockfalls artificially released from the East-side of the test slope. Therefore, we assumed that the frequency bands with the greatest energy from rockfalls would be suitable for the P-B method, as assessed by the studies of Kao (2012) and discussed at the beginning of this section. To provide the most stable estimates, after compared different width of frequency band, the top 30 highest energy frequency bands (30E) were chosen considering the most widely and less smearing information. Seismic polarization was performed by normalizing and averaging these frequency bands (30E). The

theory forming the basis of this methodology can be found in the studies of Jurkevics (1988). Moreover, the weights of rockfall N.39-impact #1 data are set to (0.20, 0.62, 0, and 0.18) for stations (TOR 1, TOR 2, TOR 3, and TOR 4), respectively. In particular, the weight for TOR 3 is 0, as the energy at this the station is lower than the noise level according to the weights defined in section 1.2.

The results of P-B are shown in Figure 5. The green point is located by only one frequency band with the maximum energy, and the cyan colour point is located by the frequency bands of 30E. From the results in this case, we found the localizations located by these two approaches are quite close to the rockfall in situ trajectory, and the marker parameter 30E is more precise and stable than when only one frequency band is applied.

1.3.2 Rectilinearity (l)

Rectilinearity (l) is a characteristic of particle motion that corresponds to the linearity of particle motion. Higher values mean that it is easier to obtain correct and precise ground motion directions. In contrast, planarity (p) indicates how the particle motion develops on a plane (Jurkevics 1988).

The degree of rectilinearity is given by Eq.7:

$$l = 1 - \frac{a_2 + a_3}{2 \times a_1}, \quad (7)$$

and the degree of planarity is given by Eq. 8:

$$p = 1 - \frac{2 \times a_3}{a_1 + a_2}, \quad (8)$$

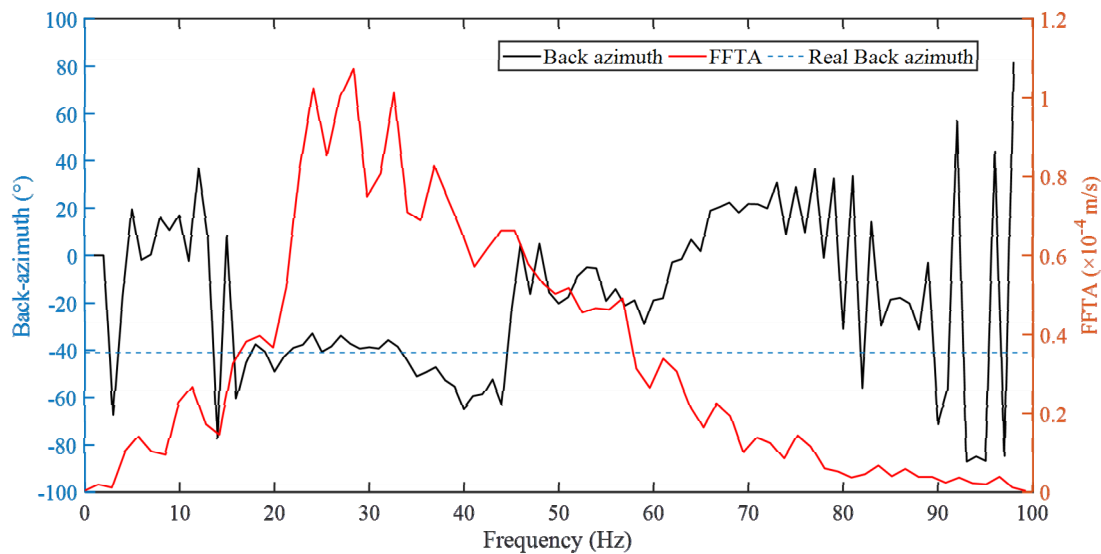


Figure 4 The correlation between back azimuths that were calculated in frequency bands of 1 Hz width and FFTA (fast Fourier transform coefficient) (i.e., the coefficients of fast Fourier transform, that representing the energy distribution in frequency) from Impact #1 of N.39 recorded by TOR 2 (the original signal is shown in Figure 2b).

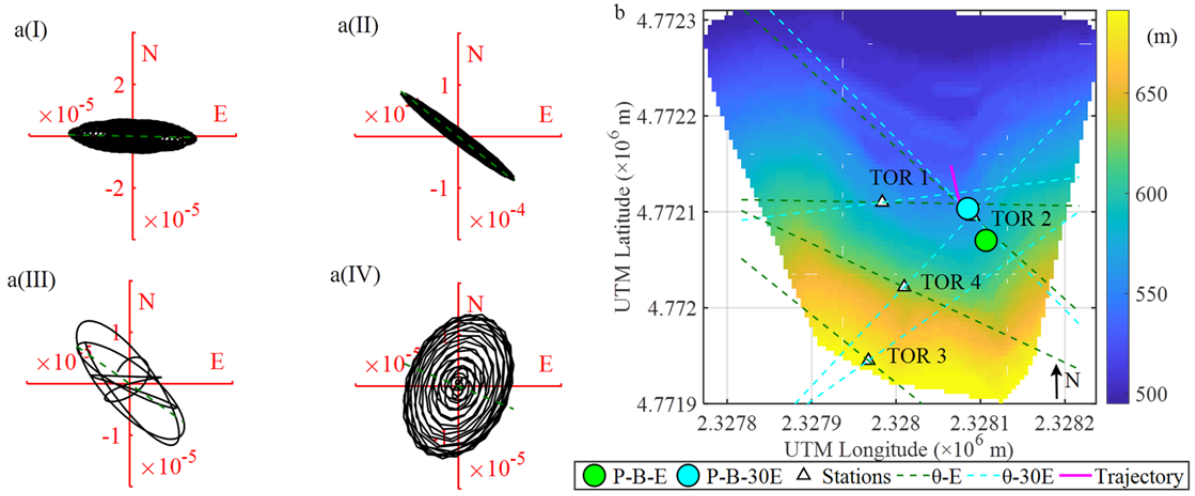


Figure 5 Panel (a): the particle motions and the back azimuths calibrated with bandpass filtered signals; in which a(I), a(II), a(III) and a(IV) are calibrated with frequency band 24 Hz – 25 Hz in TOR 1, frequency band 26 Hz – 27 Hz in TOR 2, frequency band 3 Hz – 4 Hz in TOR 3, and frequency band 17 Hz – 18 Hz in TOR 4, respectively; The rectilinearity (l) and back azimuth (θ) in a(I), a(II), a(III) and a(IV), respectively, are 0.84 , -0.9° , 0.87 , -38.4° , 0.72 , -35.3° , 0.61 , -22.5° ; Panel (b): the localization results of P-B-E and P-B-30E.

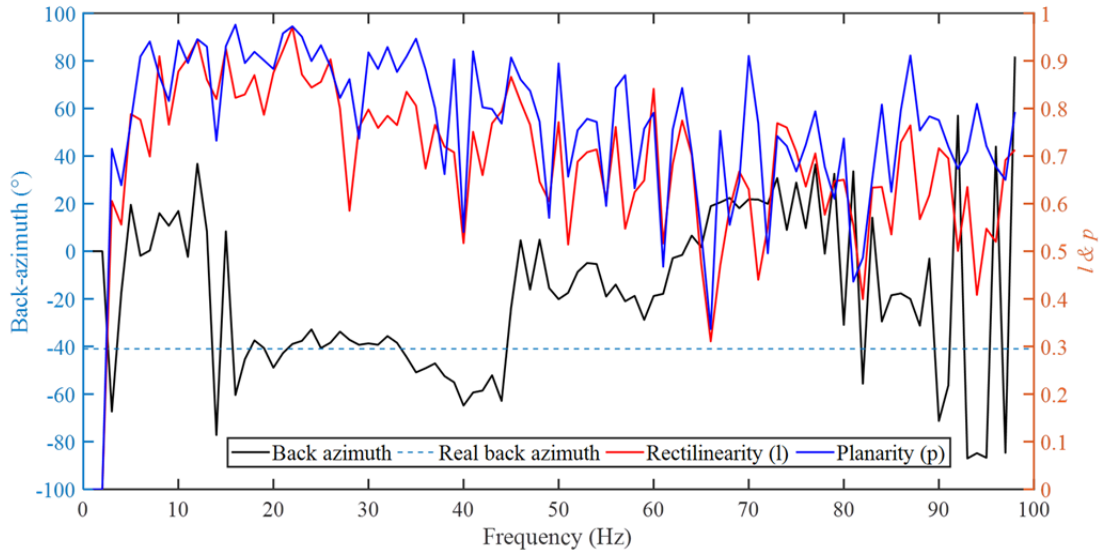


Figure 6 The correlations between back azimuths, and the rectilinearity and planarity values distributed in the frequency bands used for N.39-impact #1 in TOR 2.

where the values of $a_1 \geq a_2 \geq a_3$ are the lengths of the principle ellipsoid axes of the covariance matrix of the analysed signal in seismic polarization. When a_1 is infinitely large compared to a_2 and a_3 ($a_1 \gg a_2 \geq a_3$), then $l \approx 1$, and $p \approx 1$, i.e.; the particle motion is linear. When a_1 and a_2 are equal and infinitely large compared to a_3 ($a_1 \geq a_2 \gg a_3$), then $l \approx 0.5$, and $p \approx 1$; i.e., the particle motion moves in a plane. Finally, when a_1 , a_2 , and a_3 are equal, then $l \approx 0$ and $p \approx 0$; i.e., the particle motion moves in a sphere.

The rectilinearity and planarity values are

calculated for the 96 bandpass-filtered bands and are plotted in Figure 6 along with the calibrated back azimuths and the real back azimuths. We observe that the l and p trends do not show a significant correlation with the back azimuths. Moreover, repeating the P-B procedure to locate rockfall N.39-impact #1 by using the frequency band with the maximum rectilinearity value provides a localization result (Figure 7) from P-B- l that is not as precise as the results from either P-B-E or P-B-30E.

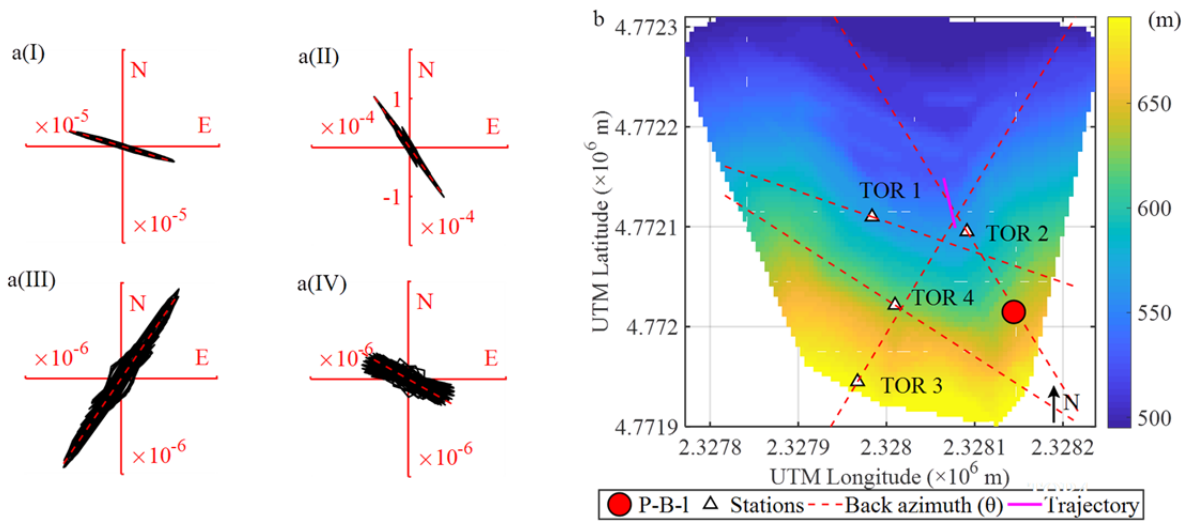


Figure 7 Panel (a): the particle motions and back azimuths calculated for each station according to the mark parameter of rectilinearity, in which a(I), a(II), a(III) and a(IV) are calibrated with frequency band 22 Hz – 23 Hz in TOR 1, frequency band 39 Hz – 40 Hz in TOR 2, frequency band 19 Hz – 20 Hz in TOR 3, and frequency band 55 Hz – 56 Hz in TOR 4, respectively; The rectilinearity (l) and back azimuth (θ) in a(I), a(II), a(III) and a(IV), respectively, are 0.97, -16.9° , 0.91, -55.0° , 0.86, 55.9° , 0.87, -29.7° ; Panel (b): the localizations obtained by means of the maximum rectilinearity procedure. The pink line indicates the real block trajectory measured in situ.

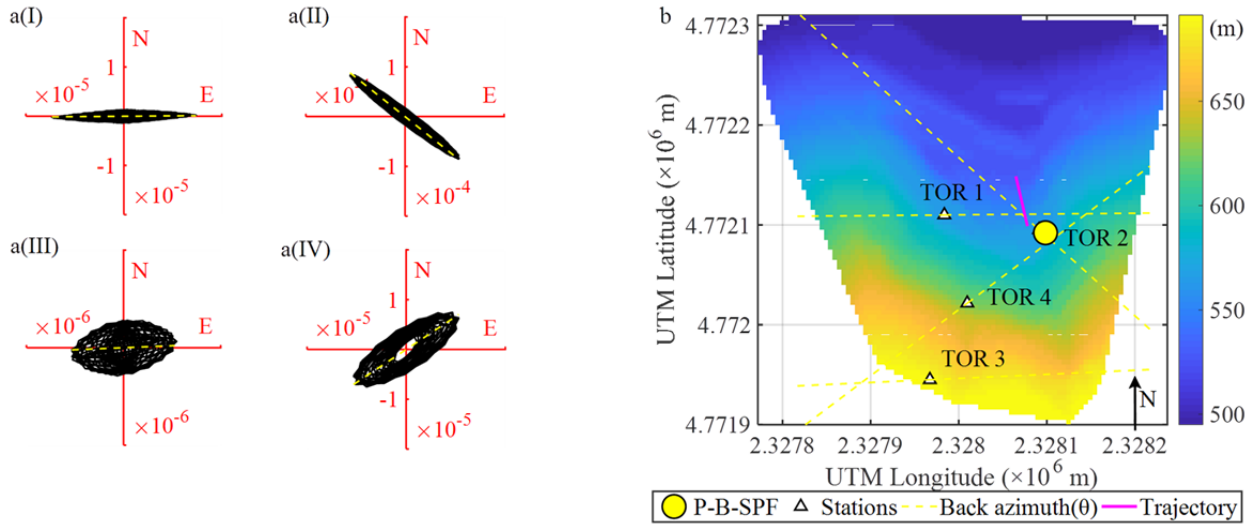


Figure 8 Panel (a): the particle motions and back azimuths calculated in each station using the permanent frequency band (SPF), in which a(I), a(II), a(III) and a(IV) are calibrated with the same frequency band 26 Hz – 27 Hz in TOR 1, TOR 2, TOR 3, and TOR 4, respectively; The rectilinearity (l) and back azimuth (θ) in a(I), a(II), a(III) and a(IV), respectively, are 0.90, 0.46° , 0.87, -38.4° , 0.59, -2.3° , 0.76, 33.5° ; Panel (b): the localization obtained by the SPF band procedure in the 26 Hz – 27 Hz band.

1.3.3 Special permanent frequency bands for all stations (SPF)

Assuming that the frequency bands created by rockfall as measured by the four stations are consistent, a special permanent frequency (SPF) band for all stations that refers to the maximum energy in the seismic station closest to the rockfall across the monitoring network was defined. For rockfall N.39, the nearest station is TOR 2, and the

most powerful frequency band is from 26 Hz to 27 Hz; hence, the SPF band for impact #1 is from 26 Hz to 27 Hz. The localization results and the particle motions of the SPF band at each station are shown in Figure 8. Results show that the localizations by means of the SPF are better than those obtained for P-B- l and are quite similar to the results obtained using P-B- E , but are not as good as those obtained by using P-B-30E.

2 Applications

When comparing the estimations of the marker parameters, the P-B-SPF and P-B-E methods are quite similar, as both methods select the frequency bands on the basis of maximum energy. The P-B-SPF method chooses the same frequency band for all seismic stations and does not consider the most powerful frequency bands recorded at the farther stations, which probably induces differences of frequency bands from the near stations because the frequency content is not only influenced by the event source but also by wave propagation. The rectilinearity marker parameter denotes particle motion, but a significant relationship between rectilinearity and the real back azimuth was not found. This finding probably means that rectilinearity is not very suitable for choosing frequency bands. Moreover, the results of marker parameter 30E, which considers the 30 highest power frequency bands, are as good as the results of the method of arrival times but avoids high accuracy onset time picks; therefore, it was suggested to apply P-B-30E for rockfalls in the following rockfall trajectory reconstructions in this study. Moreover, a similar method of frequency bands chosen according to energy can refer to the studies of Heck et al. (2019).

In the following, the method of P-B-30E was applied to three typical artificially released rockfall trajectory reconstructions (N.39, N.40, and N.15), which were characterized by different movements and three or four impacts of each block were clearly recorded by at least three seismic stations. The localization results are shown in Figure 9. The cyan circles in Figure 9a, 9c and 9e are the positions estimated by P-B-30E, and the pink points on rockfall trajectories in Figure 9 are the calibrated positions of three impacts, please note that the pink positions are not absolute coordinates measured in situ but corresponding to the observation of camera records. The grey areas in Figure 9b, 9d and 9f indicate the periods of impacts applied in seismic localization.

Rockfall N.39 is a type of sliding rockfall in which the block slides along a gentle slope that is covered by fragmented rocks, and the seismic signal shows numerous and continuous spikes. In this case, only three impacts were clearly recorded by three seismic stations and were chosen for test.

From the results, the localization results of three impacts are quite near rockfall trajectory. The errors between located positions and calibrated positions are 8 m, 31m, and 45 m of impact #1, impact #2, and impact #3, respectively.

Rockfall N.40 is also a sliding rockfall, but in this case the sliding slope was bare and smooth and was covered with a few fragmented rocks. Thus, the seismic signal shows only a few visible strong spikes. In this case, four impacts were selected for localization and are plotted in Figure 10b. From the results, all of the located positions are distributed along the rockfall trajectory. The errors of impact #1, impact #2, impact #3, and impact #4 are 13 m, 22m, 16 m, and 37 m, respectively.

Rockfall N.15 is a rebounding rockfall that took place on a steep slope and produced four clear impacts. The method of P-B-30E successfully located four impacts on the topographic map, as shown in Figure 9e and 9f, but the results are as good as rockfall N.39 and N.40, refer, in particular, to the results for P-B-30E. For the P-B-30E method, the localization errors for impact #1, impact #2, impact #3 and impact #4 are 174 m, 171 m, 90 m and 94 m, respectively.

This method was applied to all the rockfalls artificially released with clear seismic records, but only the first impacts were located. They are in totally 43 blocks, in which 24 blocks released from West-side near TOR 1 (i.e., released on a steep slope) and 19 blocks released from East-side near TOR 2 (i.e., released on a gentle slope). The released positions are marked as red points in Figure 10a, and the located results of the blocks from West-side and the located results of the blocks from East-side are marked by blue points and green points, respectively, in Figure 10. The localization results demonstrate that the blocks from West-side are located with minimum error of 2 m, maximum error of 38 m, and mean error of 15.6 m, while for blocks released from East-side the minimum error is 23 m, the maximum error is 222 m, and the mean error is 101.7 m. All the localizations are still near the monitoring network within a distance of 126 meters. The errors of all rockfalls tested are shown in Figure 10b, please note that the errors of rockfalls include maximum one-meter distance error between the released position and the real position of first impact in calculation. Besides, we can find that for all blocks

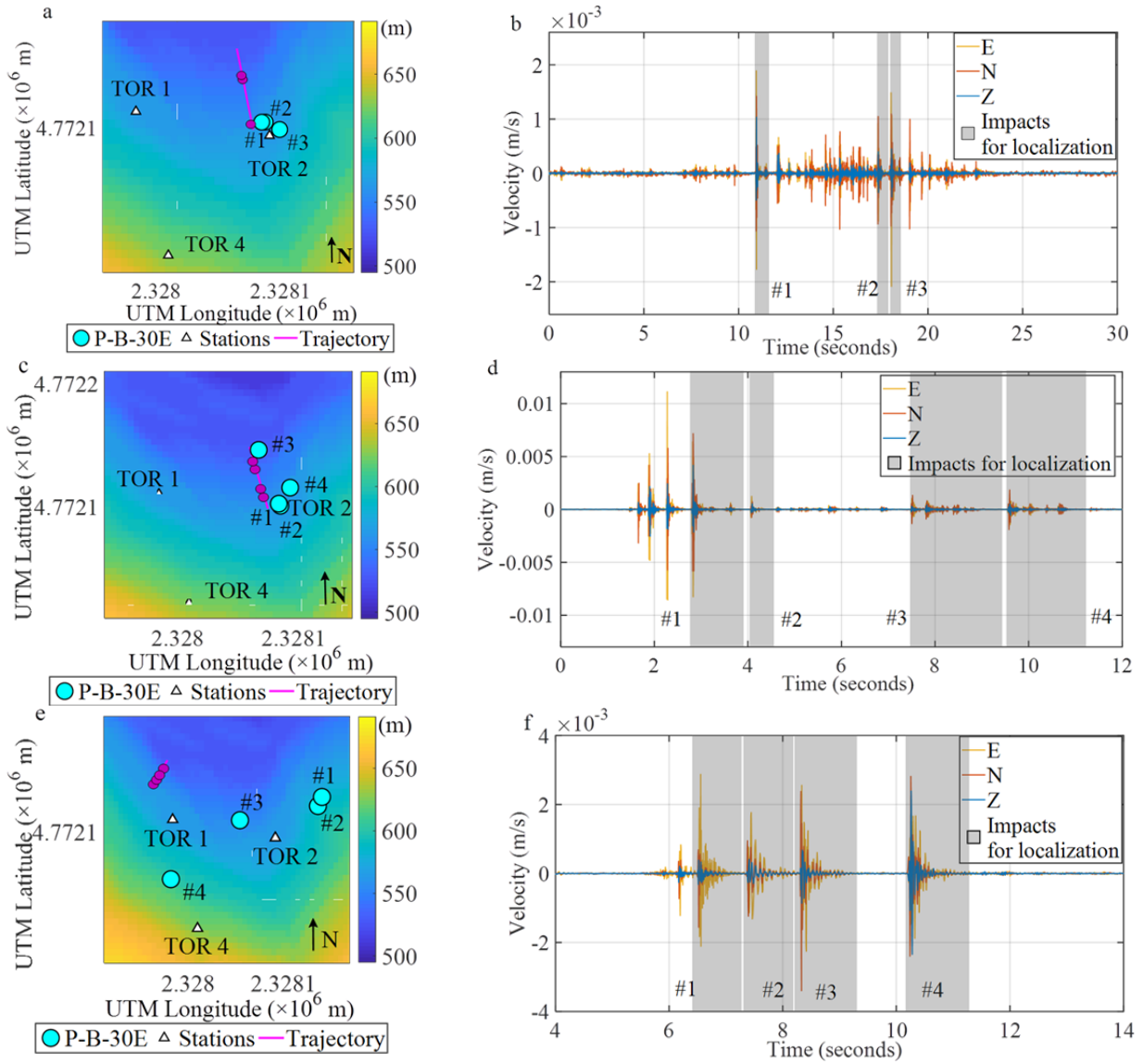


Figure 9 Localization results of rockfall N.39, N.40 and N.15: panels a, c and e): impacts localized by P-B-30E (polarization-bearing the top 30 highest energy frequency bands) (in cyan). The pink line indicates the real block trajectories as measured in situ, and the pink points on trajectories are calibrated positions—according to camera records but not the absolute coordinates measured in situ; panels b, d and f): the original signal trace with the impacts highlighted in grey.

released near station TOR 1 (released from a steep slope with clear impacts, such as rockfall N.15), the localization results are not as good as those for the blocks released near station TOR 2 (released from a gentle slope, such as rockfalls N.39 and N.40). Unfortunately, the causes of this phenomenon are still not clear. This problem likely arose from the instrument installation issues, geomorphology and the deployment of the geophone network. The slope on the west is steeper than the slope on the east, and this difference of geomorphology changed the impact angle between impactor and impacted

ground, and therefore probably changed the seismic content (e.g. the distribution of *P* and *S*-phases). Moreover, the rockfalls occurred inside the network of geophones seem to be localized more correctly.

3 Conclusions

In this study, an improved polarization-bearing (P-B) method was proposed for rockfall localization and trajectory reconstruction by using seismic monitoring. We compared three marker

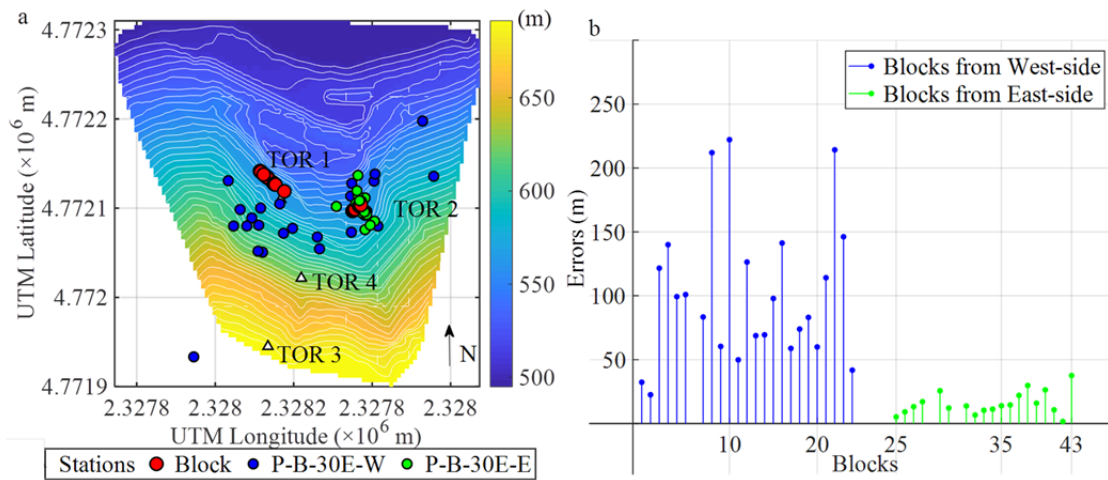


Figure 10 The localization results of artificially released rockfalls from West-side and East-side. In panel (a), the red points are the released positions, and the blue and green points are the localized positions of blocks released from West-side and East-side, respectively; in panel (b), the blue and green lines are the localization errors of blocks released from West-side and East-side, respectively.

parameters (energy, rectilinearity, and SPF) to identify the proper frequency bands for seismic polarization and back azimuth calculation. Only the energy is correlated with the correct back azimuth distributions, while the rectilinearity was uncorrelated, and the special permanent frequency band (SPF) had shortcomings for the far stations. Therefore, this study suggests that the marker parameter defined by the 30 most energy frequency bands (30E) for rockfall localization combined with an overdetermined matrix and differential assignments of weights is the best solution to calculate back azimuths when utilizing more than two stations in seismic monitoring. This approach uses the great advantage of multiple station joint mutual calibrations that consider signal quality and energy. The requirements of P-B are not as strict as the method of arrival times because P-B can be achieved by using a rough period of the signal of an event, and the proper frequency bands are indicated by the marker parameter. For this reason, the improved method makes it possible to employ automatic processing with acceptable accuracy, moreover, the location accuracy can be improved by coupling the methods of polarization and arrival times in practice. This method provides an interesting way of tracking rockfall trajectories and can also be applied to susceptible-slope area evaluations by mapping all rockfall events occurring over a long monitoring period in an early warning system (EWS).

Furthermore, since there are still some

drawbacks for this improved P-B method, additional in situ artificially released rockfall tests or a long-period monitoring case are necessary a) to evaluate the impact factors that caused the localization differences between rockfall released from a gentle slope and the rockfall released from a steep slope, b) to make analysis with more influence factors and calibrate an empirical relationship between rockfall physical properties (i.e. mass, impact speed, potential energy) and seismic signal, and c) to quantify the seismic attenuation and influence of geomorphology with more geophone networks applied.

Acknowledgements

This research was funded by the Department of Earth Sciences - University of Firenze (Italy) as part of the PRIN 2009 project– Advanced monitoring techniques for the development of early warning procedures on large rockslides (prot. 20084FAHR7_001). The devices installed were provided by Sara Electronic Instruments, and we thank the manufacturer. The seismic monitoring dataset was acquired by Alessia Lotti (from the Department of Earth Sciences - University of Firenze) during her Ph.D. work. We thank her for providing the acquired data to us and all of the people who helped to install and maintain the microseismic network. We are grateful for MATLAB technical support from Doctor Lin GAO (from the University of Firenze). Finally, the

financial supports provided by professor Nicola CASAGLI and China Scholarship Council (CSC) for Liang FENG during his study abroad in Italy, is

acknowledged. (Data applied in this study are available in PANGAEA (<https://doi.pangaea.de/10.1594/PANGAEA.912084>))

References

- Coviello V, Arattano M, Comiti F, et al. (2019). Seismic characterization of debris flows: insights into energy radiation and implications for warning. *Journal of Geophysical Research: Earth Surface*. <https://doi.org/10.1029/2018JF004683>
- Dammeier F, Moore JR, Haslinger F, Loew S (2011) Characterization of alpine rockslides using statistical analysis of seismic signals. *Journal of Geophysical Research: Earth Surface* 116(F4). <https://doi.org/10.1029/2011JF002037>
- Deparis J, Jongmans D, Cotton F, et al. (2008) Analysis of rockfall and rock-fall avalanche seismograms in the French Alps. *Bulletin of the Seismological Society of America* 98(4): 1781-1796. <https://doi.org/10.1785/0120070082>
- Feng L, Pazzi V, Intrieri E, et al. (2019) Rockfall seismic features analysis based on in situ tests: frequency, amplitude, and duration. *Journal of Mountain Science* 16(5): 955-970. <https://doi.org/10.1007/s11629-018-5286-6>
- Feng L, Pazzi V, Intrieri E, et al. (2020) Joint detection and classification of rockfalls in a microseismic monitoring network. *Geophysical Journal International*. <https://doi.org/10.1093/gji/ggaa287>
- Flinn EA (1965) Signal analysis using rectilinearity and direction of particle motion. *Proceedings of the IEEE* 53(12): 1874-1876.
- Gracchi T, Lotti A, Saccorotti G, et al. (2017) A method for locating rockfall impacts using signals recorded by a microseismic network. *Geoenvironmental Disasters* 4(1): 26. <https://doi.org/10.1186/s40677-017-0091-z>
- Guinau M, Tapia M, Pérez-Guillén C, et al. (2019). Remote sensing and seismic data integration for the characterization of a rock slide and an artificially triggered rock fall. *Engineering Geology* 257: 105-113. <https://doi.org/10.1016/j.enggeo.2019.04.010>
- Heck M, Hobiger M, Van Hervijnen A, et al. (2019) Localization of seismic events produced by avalanches using multiple signal classification. *Geophysical Journal International* 216(1): 201-217. <https://doi.org/10.1093/gji/ggy394>
- Helmstetter A, Garambois S (2010) Seismic monitoring of Séchillienne rockslide (French Alps): Analysis of seismic signals and their correlation with rainfalls. *Journal of Geophysical Research: Earth Surface* 115(F3). <https://doi.org/10.1029/2009JF001532>, 2010
- Hibert C, Mangeny A, Grandjean G, Shapiro NM (2011) Slope instabilities in Dolomieu crater, Réunion Island: From seismic signals to rockfall characteristics. *Journal of Geophysical Research: Earth Surface* 116(F4). <https://doi.org/10.1029/2011JF002038>
- Hungr O, Leroueil S, Picarelli L (2014) The Varnes classification of landslide types, an update. *Landslides* 11: 167– 194. <https://doi.org/10.1007/s10346-013-0436-y>
- Jolly AD, Thompson G, Norton GE (2002) Locating pyroclastic flows on Soufriere Hills Volcano, Montserrat, West Indies, using amplitude signals from high dynamic range instruments. *Journal of Volcanology and Geothermal Research* 118(3-4): 299-317. [https://doi.org/10.1016/S0377-0273\(02\)00299-8](https://doi.org/10.1016/S0377-0273(02)00299-8)
- Jurkevics A (1988) Polarization analysis of three-component array data. *Bulletin of the seismological society of America* 78(5): 1725-1743.
- Kao H, Shan SJ (2004) The source-scanning algorithm: Mapping the distribution of seismic sources in time and space. *Geophysical Journal International* 157(2): 589-594. <https://doi.org/10.1111/j.1365-246X.2004.02276.x>
- Kao H, Kan CW, Chen RY, et al. (2012) Locating, monitoring, and characterizing typhoon-induced landslides with real-time seismic signals. *Landslides* 9(4): 557-563. <https://doi.org/10.1007/s10346-012-0322-z>
- Lacroix P, Helmstetter A (2011) Location of seismic signals associated with microearthquakes and rockfalls on the Séchillienne landslide, French Alps. *Bulletin of the Seismological Society of America* 101(1): 341-353. <https://doi.org/10.1785/0120100110>
- Lacroix P, Grasso JR, Roulle J, et al. (2012) Monitoring of snow avalanches using a seismic array: Location, speed estimation, and relationships to meteorological variables. *Journal of Geophysical Research: Earth Surface* 117(F1). <https://doi.org/10.1029/2011JF002106>
- Lotti A, Saccorotti G, Fiaschi A, et al. (2014) Seismic monitoring of rockslide: the Torgiovanetto quarry (Central Apennines, Italy). In: Lollino, G., et al. (eds), *Engineering Geology for Society and Territory – Vol.2*, Springer International Publishing, Switzerland. pp 1537-1540. https://doi.org/10.1007/978-3-319-09057-3_272
- Lotti A, Pazzi V, Saccorotti G, et al. (2018) HVSR analysis of rockslide seismic signals to assess the subsoil conditions and the site seismic response. *International Journal of Geophysics*. Article ID: 9383189. <https://doi.org/10.1155/2018/9383189>
- Magotra N, Ahmed N, Chael E (1987) Seismic event detection and source location using single-station (three-component) data. *Bulletin of the Seismological Society of America* 77(3): 958-971.
- Moser TJ, Eck T, Nolet G (1992) Hypocenter determination in strongly heterogeneous earth models using the shortest path method. *Journal of Geophysical Research: Solid Earth* 97(B5): 6563-6572.
- Pazzi V, Morelli S, Fanti R (2019) A review of the advantages and limitations of geophysical investigations in landslide studies. *International Journal of Geophysics*. Article ID 2983087. <https://doi.org/10.1155/2019/2983087>
- Rodi W, Toksoz MN (2000) Grid-search techniques for seismic event location. Massachusetts Inst Of Tech Cambridge Earth Resources Lab.
- Rost S, Thomas C (2002). Array seismology: Methods and applications. *Reviews of geophysics* 40(3): 2-1. <https://doi.org/10.1029/2000RG000100>
- Samson JC, Olson JV (1980) Some comments on the descriptions of the polarization states of waves. *Geophysical Journal International* 61(1): 115-129.
- Vidale JE (1986) Complex polarization analysis of particle motion. *Bulletin of the Seismological society of America* 76(5): 1393-1405.
- Vilajosana I, Surinach E, Abellán A, et al. (2008) Rockfall induced seismic signals: case study in Montserrat, Catalonia. *Natural Hazards and Earth System Sciences* 8(4): 805-812. <https://doi.org/10.5194/nhess-8-805-2008>
- Xu N, Tang CA, Li H, Wu S (2011) Optimal design of microseismic monitoring array and seismic source location estimation for rock slope. *Open Civil Engineering Journal* 5(1): 36-45.
- Zhang Z, He S (2019) Analysis of broadband seismic recordings of landslide using empirical Green's function. *Geophysical Research Letters* 46:4628-4635. <https://doi.org/10.1029/2018GL081448>
- Zhang Z, He S, Li Q (2020) Analyzing high-frequency seismic signals generated during a landslide using source discrepancies between two landslides. *Engineering Geology*. <https://doi.org/10.1016/j.enggeo.2020.105640>